

Study of evanescently-coupled and grating-assisted GaInAsSb photodiodes integrated on a silicon photonic chip

Alban Gassenq,^{1,2,*} Nannicha Hattasan,^{1,2} Laurent Cerutti,³ Jean Batiste Rodriguez,³
Eric Tournié,³ and Gunther Roelkens,^{1,2}

¹Photonics Research Group, INTEC Department, Ghent University-IMEC, Sint-Pietersnieuwstraat 41, 9000 Ghent, Belgium

²Center for Nano- and Biophotonics (NB-Photonics), Ghent University, Belgium

³Institut d'Electronique du Sud (IES), UMR 5214, Université Montpellier 2 - CNRS, F-34095 Montpellier cedex 5, France

*alban.gassenq@intec.ugent.be

Abstract: In this paper we present GaInAsSb photodiodes heterogeneously integrated on SOI by BCB adhesive bonding for operation in the short-wave infrared wavelength region. Photodiodes using evanescent coupling between the silicon waveguide and the III-V structure are presented, showing a room temperature responsivity of 1.4A/W at 2.3 μ m. Photodiode structures using a diffraction grating to couple from the silicon waveguide layer to the integrated photodiode are reported, showing a responsivity of 0.4A/W at 2.2 μ m.

©2012 Optical Society of America

OCIS codes: (130.0130) Integrated optics; (040.3060) Infrared; (040.0040) Detectors.

References and links

1. B. Jalali and S. Fathpour, "Silicon photonics," *J. Lightwave Technol.* **24**(12), 4600–4615 (2006).
2. K. De Vos, I. Bartolozzi, E. Schacht, P. Bienstman, and R. Baets, "Silicon-on-insulator microring resonator for sensitive and label-free biosensing," *Opt. Express* **15**(12), 7610–7615 (2007).
3. J. T. Robinson, L. Chen, and M. Lipson, "On-chip gas detection in silicon optical microcavities," *Opt. Express* **16**(6), 4296–4301 (2008).
4. S. Stankovic, R. Jones, M. N. Sysak, J. M. Heck, G. Roelkens, and D. Van Thourhout, "1310 nm Hybrid III-V/Si Fabry-Perot Laser Based on Adhesive Bonding," *IEEE Photon. Technol. Lett.* **23**(23), 1781–1783 (2011).
5. J. G. Crowder, S. D. Smith, A. Vass, and J. Keddie, "Infrared methods for gas detection," in *Mid-Infrared Semiconductor Optoelectronics* (Springer, 2006).
6. N. Hattasan, A. Gassenq, L. Cerutti, J. B. Rodriguez, E. Tournié, and G. Roelkens, "Heterogeneous integration of GaInAsSb p-i-n photodiodes on a silicon-on-insulator waveguide circuit," *IEEE Photon. Technol. Lett.* **23**(23), 1760–1762 (2011).
7. E. M. P. Ryckeboer, A. Gassenq, N. Hattasan, B. Kuyken, L. Cerutti, J. B. Rodriguez, E. Tournié, G. Roelkens, W. Bogaerts, and R. Baets, "Integrated spectrometer and integrated detectors on silicon-on-insulator for short-wave infrared applications," accepted for oral in *Conference on Lasers and Electro-Optics (CLEO 2012)*.
8. P. Dumon, D. Taillaert, V. Wiaux, S. Beckx, B. Luyssaert, J. Van Campenhout, D. Van Thourhout, and R. Baets, "SOI Nanophotonic Waveguide structures fabricated with deep UV lithography," *Photon. Nano. Fund. Appl.* **2**(2), 81–86 (2004).
9. G. Roelkens, J. Brouckaert, D. Van Thourhout, R. Baets, R. Notzel, and M. Smit, "Adhesive bonding of InP/InGaAsP dies to processed silicon-on-insulator wafers using DVS-bis-benzocyclobutene," *J. Electrochem. Soc.* **153**(12), G1015–G1019 (2006).
10. www.hellma-analytics.com
11. www.epixfab.eu
12. D. Vermeulen, S. Selvaraja, P. Verheyen, G. Lepage, W. Bogaerts, P. Absil, D. Van Thourhout, and G. Roelkens, "high-efficiency fiber-to-chip grating couplers realized using an advanced CMOS-compatible silicon-on-insulator platform," *Opt. Express* **18**(17), 18278–18283 (2010).
13. P. Bienstman and R. Baets, "Optical modelling of photonic crystals and VCSELs using eigenmode expansion and perfectly matched layers," *Opt. Quantum Electron.* **33**(4/5), 327–341 (2001).
14. S. Bogdanov, B.-M. Nguyen, A. M. Hoang, and M. Razeghi, "Surface leakage current reduction in long wavelength infrared type-II InAs/GaSb superlattice photodiodes," *Appl. Phys. Lett.* **98**(18), 183501 (2011).
15. K. C. Nunna, S. L. Tan, C. J. Reyner, A. R. J. Marshall, B. Liang, A. Jallipalli, J. P. R. David, and D. L. Huffaker, "Short-wave infrared GaInAsSb photodiodes grown on GaAs substrate by interfacial misfit array technique," *IEEE Photon. Technol. Lett.* **24**(3), 218–220 (2012).

16. B. Kuyken, N. Hattasan, D. Vermeulen, S. Selvaraja, W. Bogaerts, W. M. J. Green, R. Baets, and G. Roelkens, "Highly efficient broadband silicon-on-insulator grating couplers for the short wave infrared wavelength range," in *Integrated Photonics Research, Silicon and Nanophotonics (IPRSN 2011)* paper IWC5 (2011).
-

1. Introduction

Silicon photonics recently emerged as an appealing platform for the integration of optical functions on a chip [1]. Originally designed toward telecommunications, sensor systems based on silicon photonics are now being developed [2,3]. The combination of silicon photonics and III-V semiconductors using a die-to-wafer bonding approach allows the integration of the full range of optical functions, including components for light emission and photodetection, on a single silicon chip. This kind of III-V integration was already demonstrated for various applications in the telecommunication window [4]. However, the short-wave (SWIR) and mid-wave (MWIR) infrared wavelength range (2-8 μm) is also attractive for several applications. In particular, the field of spectroscopic sensing exploits the strong gas/liquid/solid absorption features in this wavelength range [5]. Given its transparency window (1-4 μm), silicon photonics allows realizing integrated spectroscopic systems by combining active III-V devices on Silicon-On-Insulator (SOI) passive circuits. The availability of an integration platform for this wavelength range could enable ultra-compact, low-cost sensor solutions that outperform existing solutions by their selectivity and sensitivity. This requires the integration of short-wave and mid-wave infrared light sources and photodetectors on top of the silicon waveguide circuit. The first implementation of an integrated photodiode at 2.2 μm has recently been demonstrated [6], through evanescent coupling between the silicon waveguide and the thin-film photodiode. In this article, a detailed characterization and considerable improvement of these evanescently coupled devices is presented. Furthermore, grating-assisted photodetectors are presented, using a diffraction grating to interface the silicon waveguide with the photodetector. Since this design is more tolerant to bonding layer thickness variations, larger area bonding with high yield can be envisioned to process photodiode arrays on the outputs of large channel count SWIR or MWIR spectrometer chips [7].

2. Antimony-based photodetectors

Antimony-based materials are used for SWIR and MWIR photodetection. This material system can use 2 group V elements (Sb, As) and 3 group III elements (Ga, In, Al) to access the whole SWIR/MWIR, being lattice matched to a GaSb or InAs substrate. In this work, the GaSb-based III-V epistack has been grown by solid-source Molecular Beam Epitaxy (MBE) in a reactor equipped with both As- and Sb-valved cracker cells and conventional element-III cells. Be and Te are used as p- and n-type dopants. The substrates were on-axis (100) oriented n-type GaSb. After substrate de-oxidation at 550°C, a GaSb buffer layer is first grown at 500°C followed by 0.1 μm of InAs_{0.91}Sb_{0.09} and 0.1 μm of GaSb. These two layers will be used as etch stop layers when removing the substrate in the integration process. Then, the n-i-p junction is defined as follows. A 50nm InAs_{0.91}Sb_{0.09} and a 50nm Ga_{0.79}In_{0.21}As_{0.19}Sb_{0.81} layer are grown as the n-zone (doped 10^{18} cm^{-3}). An InAs_{0.91}Sb_{0.09} layer is chosen as n-type contact because of its narrower bandgap (0.35eV) and low contact resistance. A not intentionally doped 500nm thick Ga_{0.79}In_{0.21}As_{0.19}Sb_{0.81} layer is used for the intrinsic absorption region. The p-type region consists of 50 nm of Ga_{0.79}In_{0.21}As_{0.19}Sb_{0.81} and 50nm GaSb, both doped to 10^{18} cm^{-3} . To finish, 100nm InAs_{0.91}Sb_{0.09} is used as cap layer. Figure 1(a) shows the characterization of the epitaxial layer stack by high-resolution X-ray diffraction (HRXRD) and photoluminescence (PL) spectroscopy. HRXRD confirms a lattice-matched structure with periodic fringes showing good crystallographic quality. Indeed, a good agreement is found with the modeling for the fringes corresponding to 100nm periodicity, only the fringes related to the 700nm GaInAsSb layer cannot be accessed because the actual interfaces are not abrupt. By considering the band gap wavelength to be close to the half of the maximum PL-signal (towards longer wavelengths), it is at 2.65 μm at room temperature, which determines the cut-off wavelength of the used III-V epistack.

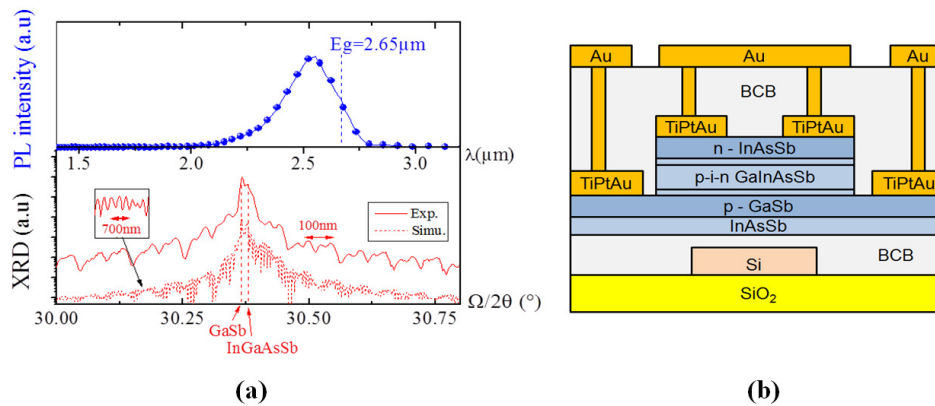


Fig. 1. (a) Photoluminescence and HRXRD measurement of the III-V heterostructure; (b) Schematic representation of the bonded epistack on a Si waveguide;

The bonded structure is schematically presented in Fig. 1(b). The process starts by the fabrication of the SOI waveguide devices with standard CMOS technology. 193nm Deep UV lithography is used for pattern definition and the waveguides are defined using ICP etching [8]. Then, an adhesive bonding technique [9] is used to integrate the epitaxial layer structure onto the SOI chip. BCB is applied on the SOI chip by spin coating. The III-V die is then attached to the chip, epitaxial layers down, and the sample is baked at 250°C during 1 hr. After the bonding process, the GaSb substrate is removed by wet etching with a HF/CrO₃ solution, until the etch stop layers are reached. These etch stop layers are removed by a tartaric and citric acid based solution (tartaric acid (5gr):H₂O:HCL:H₂O₂ 70/60/5mL and citric acid:H₂O 2:1 v/v). The mesa is formed, lithographically aligned to the underlying SOI waveguide circuit, by wet etching (citric acid:H₂O₂:H₃PO₄:H₂O 55:5:3:220 v/v). Ti(2nm)/Pt(35nm) and Au(100nm) are deposited using an e-beam evaporation system for both contacts. BCB is then spin coated on the sample and cured at 250 °C for 1 hr to passivate the device. Finally, the BCB is etched to access the top and bottom metallization with a final deposition of Ti/Au for the contact pads. This fabrication process is identical for the evanescently coupled devices and grating-coupled devices considered in this work. A 2:3 BCB(Cyclotene 3022-35):mesitylene solution was used to obtain 0.3μm BCB thickness between the III-V and the SOI.

3. Adhesive bonding for Mid-IR Photonic integrated circuits

First, the compatibility of adhesive bonding with mid-IR photonic integrated circuits was verified. In order to measure the BCB absorption in the short-wave and mid-wave infrared, absorption measurements were carried out with a Fourier Transform Infrared spectrometer (FTIR). Two methods have been used to measure the BCB absorption presented in Fig. 2. To measure low losses ($\sim\text{mm}^{-1}$) a $\sim\text{mm}$ light path was used in a QX Hellma container, which is transparent in the 1-5μm wavelength range [10]. Secondly, 1 μm of BCB spin coated on a KBr window was used for high losses measurement ($\sim\mu\text{m}^{-1}$). A good agreement is found between both measurements. Except for the high absorption peak around 3.5μm, BCB can be used as a bonding material in the 1-5μm spectral range, especially for short length scale devices such as photodetectors.

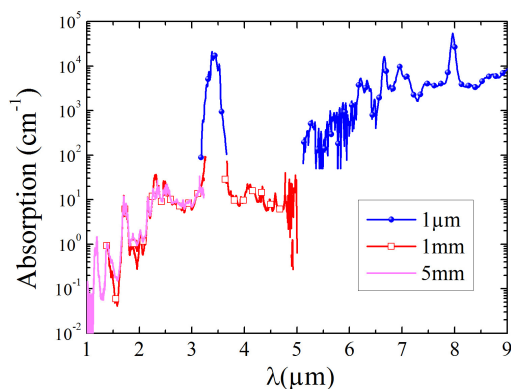


Fig. 2. BCB absorption versus wavelength measured using a Fourier Transform Infrared (FTIR) spectrometer

4. Optical coupling to a bonded photodetector

Figure 3 presents the 2D full-vectorial simulation results for the two different coupling schemes discussed in this work, using the III-V epitaxial layer stack discussed above. The first design uses evanescent coupling (design 1 on Fig. 3), which requires a thin bonding layer to obtain a high coupling efficiency ($<0.5\mu\text{m}$ in Fig. 3(c)). In this case the required photodetector length depends on the phase matching condition between the silicon waveguide mode and the modes propagating in the III-V mesa, and the actual bonding layer thickness. The second design uses a diffraction grating to interface with the III-V photodetector (design 2 in Fig. 3). Two different grating designs are presented in this work. In a first design, the grating parameters were selected such that it is compatible with the fabrication in the ePIXfab multi-project wafer scheme [11], resulting in the following parameters: $T = 1.3\mu\text{m}$, $d = 0.15\mu\text{m}$, $e = 0.15\mu\text{m}$, duty cycle = 50% and $o = 0\mu\text{m}$ with 22 periods (design 2-A). This is also the device structure that will be elaborated on in the experiments. In the second device simulation, the directivity of the grating coupler structure was optimized to obtain a maximal coupling efficiency to the thin film photodetector, resulting in $T = 0.95\mu\text{m}$, $d = 0.21\mu\text{m}$, duty cycle = 35% (defined as the ratio of the grating tooth width to the grating period) and $e = o = 0.31\mu\text{m}$ with 12 periods (design 2-B) and by adding an anti-reflection coating between the III-V structure and the BCB (thickness = $0.27\mu\text{m}$, $n = 2.42$, e.g. TiO_2). This optimized grating coupler design relies on the grating coupler structure designed in [12] for $1.55\mu\text{m}$ operation. This design was particularly geared towards a high directionality ($>90\%$). In this work all dimensions of this grating coupler design were scaled to accommodate an operation wavelength of $2.2\mu\text{m}$. The fraction of the input power that is absorbed in the GaInAsSb intrinsic region is presented in Fig. 3(c). In design 2-A, the efficiency is lower due to the limited directionality of the diffraction grating. The oscillatory behavior results from Fabry-Perot interference. In design 2-B, the absorbed power fraction is limited by the thickness of the absorption layer, since the directivity is close to 100%. Given the anti-reflection coating on the GaSb epitaxy no oscillations are observed here. It is clear that in this case much larger BCB thicknesses can be used and that a variation in the bonding layer thickness has a small influence on the resulting absorbed power fraction. This results in an easier integration process and offers a higher yield in view of the realization of large detector arrays on integrated SOI spectrometers.

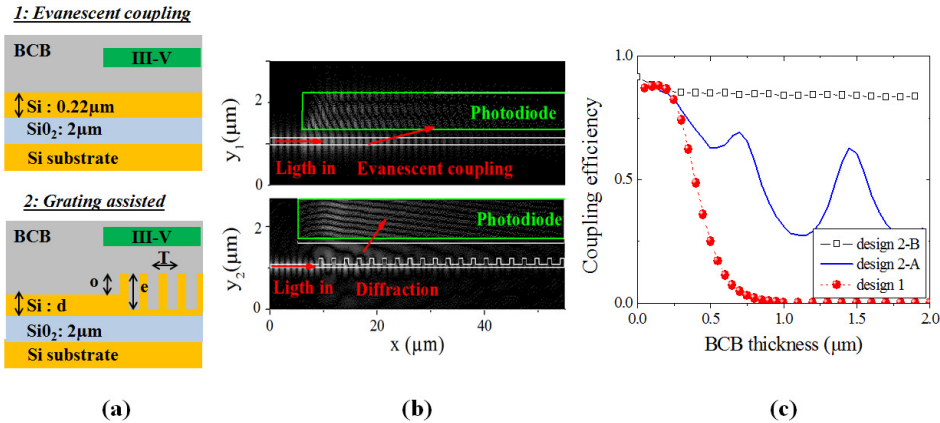


Fig. 3. Schematic representation of the considered coupling structures: (a) Side view; (b) Ez field plot of the evanescently coupled devices and devices using grating-assisted coupling (modeling using CAMFR [13]); (c) resulting absorbed power fraction as function of the BCB thickness for design 1, 2-A and 2-B.

5. Evanescent coupling photodetectors

Previously, a responsivity of 0.35A/W at room temperature [6] in evanescently coupled devices was reported. In this work, we report a substantial improvement in the detector responsivity and we investigate the electrical properties of these devices by assessing the influence of the mesa size and the operation temperature on the current versus voltage curve. Figure 4 presents the top view and cross-section of an integrated photodiode using evanescent coupling.

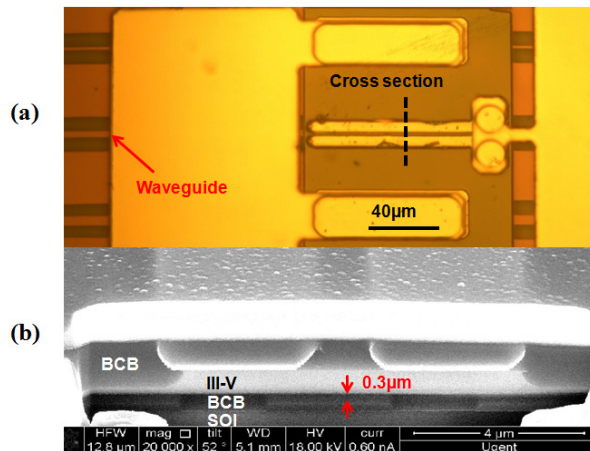


Fig. 4. SWIR integrated photodiodes using evanescent coupling to couple light from the waveguide to the photodiode: (a) top view; (b) SEM cross section

Figure 5(a) shows the system responsivity S defined by the ratio between the optical power at the fiber input and the photocurrent. A grating coupler structure was used to interface the optical fiber to the silicon chip. A Cr:ZnSe laser was used to characterize the system from 2.05 to 2.4 μm wavelength and a III-V semiconductor tunable laser was used for characterization between 1.6 to 1.7 μm. In a wavelength band around 2.2 μm the diffraction grating excites the TE mode in the silicon waveguide with a maximal efficiency of -10dB. The maximum system responsivity lies around 2.2 μm, which was the targeted operation wavelength for the fabricated detectors. According to the grating coupler efficiency G used to

inject light in the waveguide presented on Fig. 5(b), the waveguide-to-detector responsivity is plotted in Fig. 5(c) with the intrinsic maximum value $R_{\max} = q/h\nu$ and the corresponding minimum waveguide-to-detector coupling efficiency indicated on the graph (assuming 100% carrier collection efficiency). In all of these experiments the detector was reverse biased at $-1V$ and measurements were carried out at room temperature. From these measurements, a responsivity of $1.4A/W$ is obtained at $2.3\mu m$, illustrating the efficient optical coupling and carrier collection in the photodetector. The improvement in responsivity compared to [6] is due to better alignment between the waveguide and the photodiode, as presented in Fig. 4. In addition, the grating coupler can be used to inject TM light into the Si waveguide centered around $1.65\mu m$. In this wavelength range, the responsivity is $0.3A/W$ because of a lower evanescent waveguide-to-detector coupling efficiency at shorter wavelengths. These measurements show the feasibility of a broadband integrated detector (at least from 1.6 to $2.3\mu m$) with an GaInAsSb bulk absorption region.

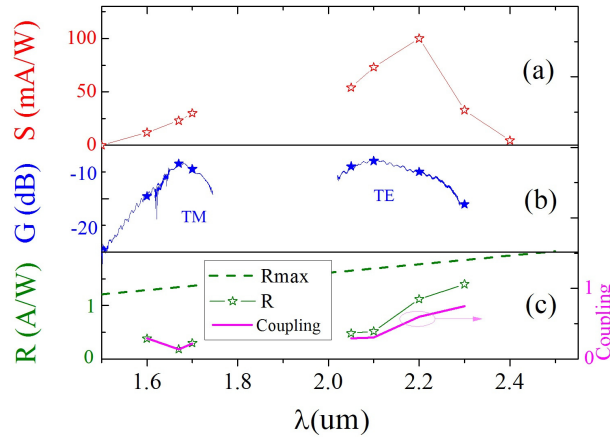


Fig. 5. (a) system responsivity ($S = I_{\text{photo}}/P_{\text{fiber}}$); (b) grating coupler efficiency and (c) deduced intrinsic photodiode responsivity and minimum evanescent coupling efficiency as a function of wavelength

In order to improve the sensitivity of the devices, which is limited by the photodiode dark current [6], the low temperature operation of the device was assessed. Figure 6(a) presents the current density versus voltage curve as a function of temperature. At room temperature, the R_0A is $0.1\Omega cm^2$ and the dark current density at $-1V$ is $0.3A/cm^2$ for a device with a mesa size of $60\mu m$ by $10\mu m$. At liquid nitrogen temperatures, the dark current density is reduced to $60\mu A/cm^2$. This dark current reduction is limited to 4 orders of magnitude because of the strong surface leakage current which will be quantified in Fig. 6(b). Characterizations were also performed after a thermal cycling between room temperature and liquid nitrogen temperature showing no degradation in photodiode responsivity or dark current. This shows that BCB adhesively bonded III-V/silicon photodetectors can be used at liquid nitrogen temperatures, which substantially enhances their noise equivalent power. The influence of the mesa size on the dark current is presented in Fig. 6(b), showing the dark current at $-0.1V$ at room temperature as a function of the perimeter to surface ratio (P/S) of the mesa. On this graph two fabrication processes with the same bonded epi-stack are compared. The first process is using a test contact mask on the left side of the graph; it contains results for various mesa sizes with and without BCB passivation. The comparison between BCB passivation (star dots) and without passivation (square dots) shows an important improvement of the dark current by using a BCB passivation process. The right side of the graphic shows the dark current of the integrated photo-detectors, with BCB passivation, which are in line with the device run using the test mask.

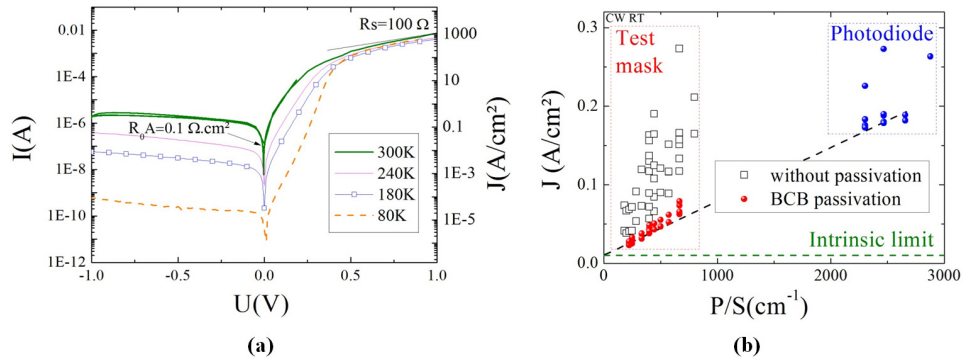


Fig. 6. Photodiode leakage study: (a) I(V) curve as a function of temperature; (b) dark current density at -0.1V as a function of the perimeter to surface ratio (bonded device structure)

By fitting all data, we find a good agreement between both processes to obtain the intrinsic dark current density related to the epi-stack, which is very low ($\sim 10\text{mA}/\text{cm}^2$). Furthermore, we can see that 95% of the photodiode dark current in the integrated devices comes from sidewall leakage. Different passivation methods can be used, e.g. using SiO_2 [14] or SU8 [15] to reduce the surface leakage further. Given the large surface leakage current, mesa shape optimization is of paramount importance to further enhance the sensitivity of the device. Since diffraction grating based devices can be made smaller and have a form factor closer to 1 (and hence have a lower perimeter/surface ratio) than evanescently coupled devices, these devices will be studied in the next section.

6. Grating-based photodetectors

Given the advantages of grating-based photodetectors, both in terms of a more tolerant integration process and its potentially smaller footprint, the first demonstration of a grating-assisted photodiode at $\lambda = 2.2\mu\text{m}$ using a grating coupler as a coupling element between the waveguide and the photodiode is presented. In this case, the photodiode mesa is still $50\mu\text{m}$ long and $20\mu\text{m}$ wide, to be larger than the Mid-IR grating coupler used in the experiment [16]. The device footprint can however be substantially reduced by reducing the grating coupler dimensions, as was illustrated in Fig. 3 (design 2-B), leading to a $12\mu\text{m}$ long device. Figure 7(a) presents the current versus voltage curve for various fiber-launched power levels and a SEM cross section/top view picture of the integrated photodiode is shown in Fig. 7(b). The photodiode dark current is in the same range as in the evanescently coupled devices, around $-4\mu\text{A}$ at -1V corresponding to $0.4\text{A}/\text{cm}^2$ at room temperature. The system responsivity (input fiber power to photocurrent ratio at -1V), is $25\text{mA}/\text{W}$. Given the measured input grating coupler efficiency of -12dB , we can deduce an intrinsic detector responsivity of about $0.4\text{A}/\text{W}$. This value is lower than for evanescently coupled devices because the III-V structure intrinsic absorption region thickness is not sufficiently thick for surface normal operation and because of the limited directionality of the diffraction grating. However, with this design, the photodiode can operate with a thicker BCB layer (design 2-A and 2-B on the Fig. 3(c)). This results in a more relaxed fabrication process, which is expected to result in a higher yield integration process for the integration of large arrays of photodiodes on SOI spectrometer circuits [7].

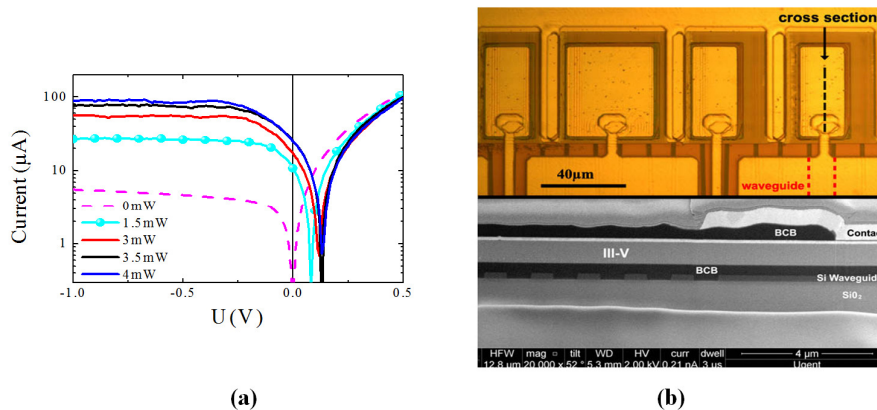


Fig. 7. SWIR integrated photodiodes using a grating coupler to couple light from the waveguide to the photodiode: (a) $I(V)$ as function of the optical power in the fiber; (b) top view and SEM cross section

7. Conclusion

GaInAsSb photodiodes integrated on a silicon waveguide circuit for operation in the $2.2\mu\text{m}$ wavelength range are reported. Devices using evanescent coupling show a high coupling efficiency between the waveguide and the photodiode resulting in a responsivity of 1.4A/W and a minimum dark current density under 0.3A/cm^2 at -1V . Grating coupler based devices show a responsivity of 0.4A/W and a dark current density of 0.4A/cm^2 . Simulations indicate however that grating coupler based devices can match and perhaps exceed beyond the performance of evanescently coupled devices. Based on this technology, GaInAsSb based photodetector structures and hence integrated spectrometric functions are now developed as a next objective at $2.2\mu\text{m}$ wavelength, and can be envisioned to cover the whole SOI long-wavelength transparency region, up to $4\mu\text{m}$.